Optica Applicata, Vol. XXIV, No. 1–2, 1994

Studies of some mechanical properties of the human tibia by holographic interferometry

E. JANKOWSKA-KUCHTA, H. KASPRZAK

Institute of Physics, Technical University of Wrocław, Wybrzeże Wyspiańskiego 27, 50–370 Wrocław, Poland.

M. FECHNER

Institute of Legal Medicine, University of Münster, Münster, Germany.

G. VON BALLY

Laboratory of Biophysics, Institute of Experimental Audiology, University of Münster, Münster, Germany.

A double exposure interferometry method has been applied to investigate the mechanical properties of human tibia under oblique bending. The bone rigidity G and Young's modulus E have been calculated from the obtained interferograms. The results are compared with Young's modulus values $E = 7-18$ GPa obtained by other authors.

1. Introduction

The orthopaedist deals with many solid structures. They may be composed of biological materials such as bone and cartilage. The most important is a precise knowledge of the properties of these materials under loading conditions encountered in the human body. They may be characterized by mechanical parameters such as Young's modulus (elasticity modulus) E, rigidity G and the area moment of inertia.

There have been a number of studies over the last decade devoted to the determination of the elastic properties of the bone. Some of them used holographic interferometry [1], [2]. However, they applied holographic interferometry to qualitative analysis of deformations of bones [3] or skulls [4].

The purpose of this work is to present the holographic interferometry method applied to determine elastic modulus of the human tibia. The results are compared with the elastic modulus values obtained by other authors [5].

2. Experiment

The object of our interest and measurement is a human tibia obtained from a white male a few hours *post mortem* and immersed in formalin for 48 hours. After that time it was carefully cleaned of all soft tissuue and bone marrow. The clean and dry tibia was placed on cylindrical holders mounted on an antivibrational table.

According to EVANS [6] the difference in Young's modulus between dead and living bone is negligible, so the dead bone has been chosen for this experiment (assuming this does not affect results).

Using holographic interferometry (double exposure technique) the bone deflection has been recorded. In double exposure technique, two holograms are recorded on the same holographic plate, for two different values of the bending moment. When reconstructed, the two holographic images interfere with one another and the resulting interferogram image shows fringes representing the deflection. The bone undergoes a bending process by applying force in the middle of it. For different interferograms the differential load between two exposures was in the range of 4–5 N, which allowed obtaining sufficient fringe density. Increase of the loading force was applied within about half a second and the time interval between two exposures was 5 s. The value of the preload was equal to 50 N. The measured bone length was limited by the cylindrical holders and was equal to 126 mm (Fig. 1). Figure 2 presents a holographic system used in this experiment. The argon laser at a wavelength of 514 nm and output power of 500 mW was used as a light source. The bone was illuminated from the top by the fiber bundle and the light scattered by the bone surface was directed to the recording plane by a big mirror placed above the bone. The bending force acted in the same direction as the illuminating beam. Holograms were recorded using the Rottenkolber photothermoplastic camera.

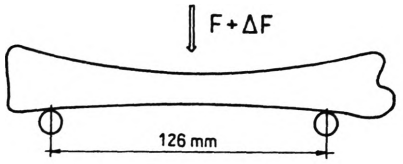

Fig. 1. Loading system. F – bending force

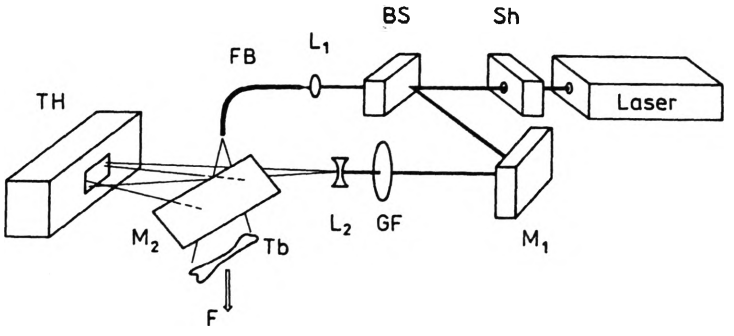

Fig. 2. Optical arrangement. Sh – shutter, BS – beam splitter, FB – fibre bundle, GF – gray filter, L_1, L_2 – lenses, M_1, M_2 – mirrors, TH – thermoplastic plate, F – bending force, Tb – human tibia

Because of the asymmetry of the bone's cross-section, the interferograms were recorded for three different force orientations in respect of the cross-section of the

bone, as shown in Fig. 3. It means that, after a series of recording the interferograms, the bone was turned around its longitudinal axis and the next series of interferograms were recorded. In all the cases the force acted in the cross-section plane, placed in the middle of the bone and perpendicular to the longitudinal bone axis. Figure 4 shows the examples of two interferograms recorded for two different orientations of the bending force. The interference fringes correspond to the bone deflection.

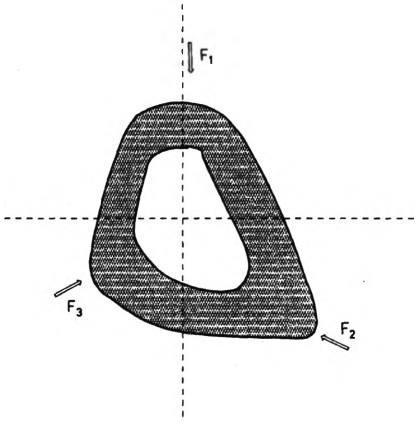

Fig. 3. Three different directions of loading force in the middle plane of the bone cross-section

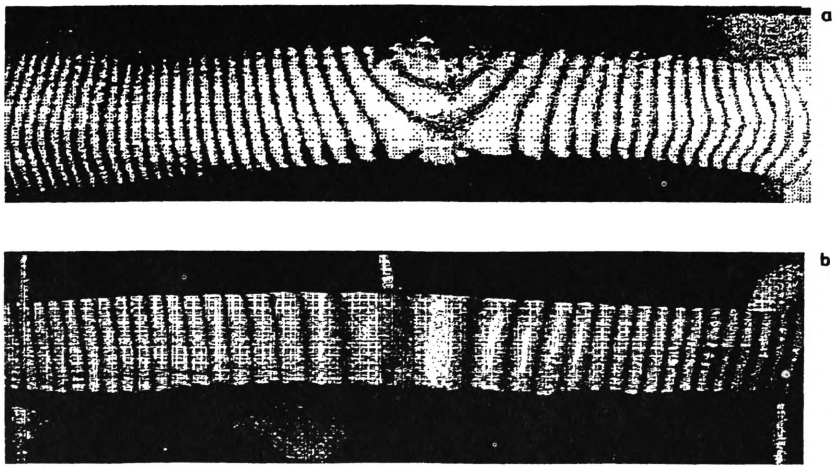

Fig. 4. Example of holographic interferograms for two different orientations of bending force in respect of the bone cross-section

After recording all of the interferograms, the bone was cut through the middle in direction perpendicular to the longitudinal bone axis. Then, the cut and polished cross-section of the bone was photographed. The photographs obtained were used to calculate the geometrical parameters of the bone's cross-section.

3. Analysis

Knowing the value of displacement d between neighbouring fringes, equal to $\lambda/2 = 257$ nm, and the fringe number at the fixation points $N = 0$, the diagrams of the bone deflection $p(x)$ as a function of the bone length have been obtained. The deflection p, measured directly from the holographic interferograms, presents the projection of the total displacement w on the loading direction.

The last-square method was used for numerical approximation of the experimental deflection data obtained from holographic interferograms by means of a polynomial. The interferograms were scanned by HP ScanJet Plus scanner and the position of the fringe centres along the longitudinal axis of the bone were taken into account.

An example of the polynomial least-square approximation used to analyze the experimental data is presented in Appenxix I. In all cases of the analyzed interferograms, the 4th order polynomial showed a very good approximation of the experimental data and was taken for further calculations.

Since the deformation between all inner points of the bone can be neglected, the rigidity can be described as for a beam loaded in the middle. In the general case, the differential deflection equation of the bending beam is

$$\frac{d^2w(x)}{dx^2} = \frac{M(x)}{EI(x)} \tag{1}$$

where: $w(x)$ – beam deflection, $M(x)$ – bending moment, $I(x)$ – area moment of inertia of the beam cross-section, E – Young's modulus, x – coordinate along the beam longitudinal axis.

Because of the bone asymmetry, mentioned previously, the load direction and the principal axes are different. In that case, the oblique bending must be considered and the Eq. (1) must be changed into a set of two equations, where the components of the bone deflection (projection of the deflection vector on the principal axes) were used:

$$\frac{d^2v}{dx^2} = \frac{M_z(x)}{EI_y(x)}, \tag{2a}$$

$$\frac{d^2u}{dx^2} = \frac{M_y(x)}{EI_z(x)}, \tag{2b}$$

where: u, v – components of the total displacement vector on the principal axes, $I_z(x)$, $I_y(x)$ – principal moments of inertia of the cross-section area, $M_y(x)$, $M_z(x)$ – components of the bending moment on the principal axes.

The area and the principal moments of inertia of the bone's middle cross-section were calculated numerically from its scanned photography.

The area of cross-section was divided into 1000 elementary subareas, and the computer program determined the total area, position of its centre and the respective principal moments of inertia. Knowing the values of those moments and the position of the cross-section in a chosen coordinate system, the following equation may be used to find the orientation of the neutral axes:

$$\tan\psi = \frac{I_z(x)}{I_y(x)}\operatorname{ctan}\varphi \tag{3}$$

where: φ – angle between load direction and the principal axis, ψ – angle between the principal axis and the neutral axis.

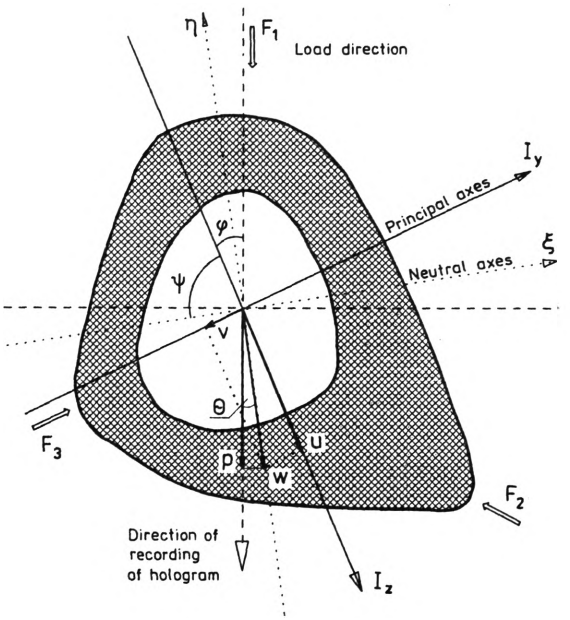

Fig. 5. Tibia cross-section coordinate system and the definition of the parameters

The tibia cross-section in the bone middle point is presented in Fig. 5, the orientation and definition of the geometric parameters are indicated. After introducing the parameter k

$$k = I_z/I_y, \tag{4}$$

and the polar moment of inertia

$$I_0 = I_z + I_y, \tag{5}$$

the principal moments of inertia can be expressed as

$$I_y = \frac{I_0}{k+1} \tag{6}$$

and

$$I_z = \frac{I_0 k}{k+1}. \tag{7}$$

For all interferograms the fourth order polynomial describes the measured deflec-

tion diagram with a very good accuracy. The use of the higher order polynomial (fifth and sixth) as shown in Appendix I does not increase the accuracy of approximation. The polynomial has the following form:

$$p = a+bx+cx^2+dx^3+ex^4. \tag{8}$$

From the geometry presented in Fig. 5 one gets

$$p = w\cos\theta = \sqrt{u^2+v^2}\cos\theta \tag{9}$$

where θ – angle between load axis and the direction of the total displacement.

The components of bending moment caused by the loading increase between two exposures may be expressed as:

$$M_z = \Delta F x\cos\varphi, \tag{10a}$$
$$M_y = \Delta F x\sin\varphi \tag{10b}$$

where ΔF – bending force.

Applying Equations (10), (6), (7) to Equations (2a) and (2b) gives:

$$\frac{d^2v}{dx^2} = \frac{\Delta F\cos\varphi\cdot x(k+1)}{EI_0(x)}, \tag{11a}$$
$$\frac{d^2u}{dx^2} = \frac{\Delta F\sin\varphi\cdot x(k+1)}{EI_0(x)k}. \tag{11b}$$

From Figure 5 one can deduce the following relations between the variables w, u, v, p, φ, θ:

$$w\cos\theta = p,$$
$$u = w\cos(\varphi-\theta) = \frac{p}{\cos\theta}\cos(\varphi-\theta), \tag{12}$$
$$v = w\sin(\varphi-\theta) = \frac{p}{\cos\theta}\sin(\varphi-\theta).$$

Using them, the following equations can be written:

$$\frac{d^2v}{dx^2} = \frac{d^2}{dx^2}\left(p\frac{\cos(\varphi-\theta)}{\cos\theta}\right), \tag{13a}$$
$$\frac{d^2u}{dx^2} = \frac{d^2}{dx^2}\left(p\frac{\sin(\varphi-\theta)}{\cos\theta}\right). \tag{13b}$$

For the next transformation the assumption that the angles φ and θ do not change significantly along the x-axis has been made. This allows us to rewrite (13) as:

$$\frac{d^2v}{dx^2} = \frac{\cos(\varphi-\theta)}{\cos\theta}(2c+6dx+12ex^2), \tag{14a}$$
$$\frac{d^2u}{dx^2} = \frac{\sin(\varphi-\theta)}{\cos\theta}(2c+6dx+12ex^2). \tag{14b}$$

Combining Equations (11) and (14), one obtains:

$$EI_0(x) = \frac{M_z(x)(k+1)}{d^2v/dx^2} = \frac{(k+1)x\Delta F\sin\varphi\cos\theta}{(2c+6dx+12ex^2)\cos(\varphi-\theta)}, \tag{15a}$$

$$EI_0(x) = \frac{M_y(x)(k+1)}{(d^2u/dx^2)k} = \frac{(k+1)x\Delta F\sin\varphi\cos\theta}{(2c+6dx+12ex^2)\sin(\varphi-\theta)k}. \tag{15a}$$

From these equations the rigidity $G(EI_0)$ and Young's modulus in the middle point of the cross-section of the human tibia have been calculated.

4. Results

The calculation of Young's modulus from Equations (15a) and (15b) gives two values (E' and E'') of the averaged elastic modulus in the bending test, for each force orientation. The Table presents the calculated averaged Young's modulus for three different force orientation, as well as the respective averaged rigidity G.

Table

A [cm^2]	I_y [cm^4]	I_z [cm^4]	E' [GPa]	E'' [GPa]	G' [Nm^2]	G'' [Nm^2]
2.06	1.11	0.78	7.7	9.1	145.5	171.7
			11.8	11.8	223.5	223.8
			12.6	14.2	238.2	269.1

5. Discussion

Van BUSKIRK and ASHMAN [5] reported simular data for the human tibia. Comparison between their data and results presented in this paper shows that Young's modulus values are in agreement with their values. KASPRZAK and PODBIELSKA [3] investigated the human tibia rigidity and the results presented in their paper are in full agreement with our results. PIZIALI *et al.* [7] and MILLER and PURKEY [8] measured the tibia cross-sectional area and the tibia principal moment of inertia. Our results correspond with the latter paper, and they are a little bit smaller when compared with the former one.

The most important result presented in this paper is the possibility of using the holographic interferometry method for nondestructive measurement of the human tibia Young's modulus and the rigidity. One should mention that, according to the bone anisotropy and unhomogeneity, the measured modulus presents some average value along the bone axis. The values obtained were calculated for one cross-section – in the middle of the bone, but the similar elastic modulus in the bending test for the whole bone can easily be predicted knowing the change of the area moment of inertia along the bones's longitudinal axis, the function describing the bone deflection along that axis, and the direction of loading. Also this paper shows the dependence between the cross-section principal moments of inertia values (related to

the shape of the bone) and the angle θ introduced in Eq. (9). It turned out that if the ratio of the principal moments of inertia $k = 1.4$, the $\cos\theta = 0.986$, so the deflection p, which is used to determine value E, introduces less than a 2% error into the calculation. Because of that the right side derivative in Eqs. (14a) and (14b) can be calculated assuming independence of θ and φ on x. Our calculations are presented in Appendix II.

Even with that assumption our results are in agreement with the values obtained in different techniques and the differences are mostly due to:

1. Differences of bones from different individuals, which may depend on several variables (weight, height, sex, *etc.*).

2. Small changes in bone elasticity connected with drying (the time interval between bone preparation and the measurement).

3. Different load values – in our method the stresses are low, in traditional stress-strain experiment, loads are much bigger.

No attempt has been made to account for changes in bone density. The bone was considered to be uniform and homogeneous for these calculations in a similar way as did LEVIS [9], PIOTROWSKI and WILCOX [10], RYBICKI *et al.* [11].

Summing up, one can conclude that the application of holographic methods can support and complement other biomechanical techniques.

Appendix I

This Appendix presents an example of the polynomial least-square approximation applied to determine the deflection of the bone, recorded on the holographic interferogram shown in Fig. 5a. Figure I1 shows the experimental data points representing the centres of the fringes and third order polynomial approximation in the form

$$F_3(x) = a_3 + b_3 x + c_3 x^2 + d_3 x^3 \tag{I1}$$

with the coefficients:

$$a_3 = -0.18020203, \qquad b_3 = 0.13249724,$$
$$c_3 = -0.00106867, \qquad d_3 = 3.42773278.$$

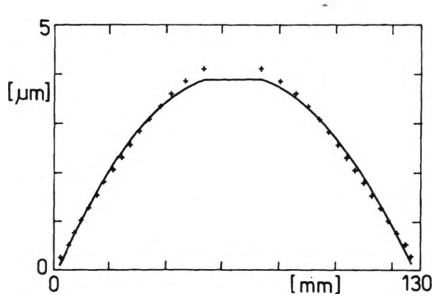

Fig. I1. Deflection diagram as a function of the bone length. + + + experimental points, —— analytical fit (third order polynomial)

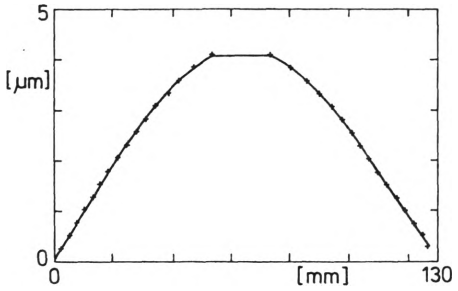

Fig. I2. Deflection diagram as a function of the bone length. + + + experimental points, —— analytical fit (fourth order polynomial)

Figure I2 shows the same experimental data points and fourth order polynomial:

$$F_4(x) = a_4 + b_4 x + c_4 x^2 + d_4 x^3 + e_4 x^4 \tag{I2}$$

with the coefficients:

$a_4 = 0.03087475,$
$b_4 = 0.09082546,$
$c_4 = 0.00057086,$
$d_4 = -0.00002031,$
$e_4 = 8.13228017 \cdot 10^{-8}.$

The polynomial coefficients calculated for fifth and sixth order polynomials are respectively equal to:

$a_5 = 0.02035045$
$b_5 = 0.09394257$
$c_5 = 0.00038317$
$d_5 = -0.00001621$
$e_5 = 4.4430421 \cdot 10^{-8}$
$f_5 = 1.16695288 \cdot 10^{-10}$

and

$a_6 = -0.00697457$
$b_6 = 0.10657675$
$c_6 = -0.00076093$
$d_6 = 0.00002269$
$e_6 = -5.52033894 \cdot 10^{-7}$
$f_6 = 4.31696817 \cdot 10^{-9}$
$g_6 = -1.10694618 \cdot 10^{-11}$

The integral along the bone length in the form

$$C(n) = \int_0^{126} [F_{n+1}(x) - F_n(x)]^2 dx \tag{I3}$$

where $n = 3, 4, 5$ was chosen to determine the goodness of the polynomial fitting. The integrals calculated for higher order polynomial approximation give

$$\int_0^{126} [F_4(x) - F_3(x)]^2 dx = 1.77168774,$$

$$\int_0^{126} [F_5(x) - F_4(x)]^2 dx = 0.0302215,$$

$$\int_0^{126} [F_6(x)-F_5(x)]^2 dx = 0.0378981.$$

It can be seen that the difference between values of the integral (I3) for fourth and fifth polynomial orders is more than two orders of magnitude smaller than the difference between the respective third and fourth orders, and almost the same as between fifth and sixth.

Therefore, the fourth order polynomial was used to approximate the experimental deflection points. Higher order polynomials do not increase the accuracy of the approximation.

Appendix II

In double-exposure holographic interferometry, the interference fringes represent the displacement of the tested object in the direction perpendicular to the holographic plate. Because of the asymmetry of the bone cross-section and its variable geometry along the longitudinal bone axis, the direction of the bone's total displacement w and the displacement p recorded on the interferogram may not lie on one line. Both directions form the angle θ, as shown in Fig. 5 where the angle dependence is as follows:

$$\theta = \varphi + \psi - 90°. \tag{II1}$$

The ratio p/w can be rewritten as follows:

$$\frac{p}{w} = \cos\theta = \cos(\varphi+\psi-90°) = \cos\left[\varphi + \arctan\left(\frac{I_z}{I_y}\operatorname{ctan}\varphi\right) - 90°\right]$$
$$= \sin\left[\varphi + \arctan\left(\frac{I_z}{I_y}\operatorname{ctan}(\arctan(\sqrt{k}))\right)\right]. \tag{II2}$$

It shows the correlation between the shape of the bone cross-section (I_z/I_y), total displacement w and the displacement p, recorded in the holographic method. From the condition on extremes of the function (II2), the maximum difference between the total and measured displacements as a function of angle θ can be determined

$$\frac{d(\cos\theta)}{d\varphi} = \cos(\varphi + \arctan(k\operatorname{ctan}\varphi))\left(1 - \frac{k(1+\operatorname{ctan}^2\varphi)}{1+k^2\operatorname{ctan}^2\varphi)}\right) = 0. \tag{II3}$$

In order to satisfy the above equation, the following conditions should be fulfilled:

$$\cos(\varphi + \arctan(k\operatorname{ctan}\varphi)) = 0, \tag{II4}$$

or

$$1 - \frac{k(1+\operatorname{ctan}^2\varphi)}{1+k^2\operatorname{ctan}^2\varphi} = 0. \tag{II5}$$

1. For $k = 1$, any angle φ gives $\cos\theta = 1$, it means that for the circular cross-section ($I_z/I_y = 1$) the direction of the total displacement coincides with the direction of measured displacement.

2. For $k \neq 1$, Equation (II5) leads to the condition

$$\varphi_{min} = \arctan(\sqrt{k}) \tag{II6}$$

where φ_{min} denotes the angle between the force and the principal axis direction, for which the values of the total displacement component p of the given total displacement vector w reaches its minimum.

So, the minimum ratio p/w is equal to

$$\cos\theta_{min} = \cos(2\arctan(\sqrt{k}) - \pi/2). \tag{II7}$$

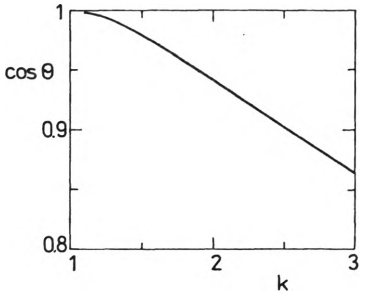

Fig. II1. Dependence between parameter k and $\cos\theta$

Figure II1 shows the graph of the function (II7). The values of k in the central cross-section of the examined bone amounted to 1.42. It corresponds to the angle $\varphi_{min} = 49.79°$ and the minimum value of $\cos\theta_{min} = 0.986$.

The results show that the accuracy in determination of the bone displacement during the experiment is about 2% in the middle of the bone (where $k = 1.42$).

References

[1] KASPRZAK H., PODBIELSKA H., SULTANOVA N., Acta Polytech. Scand. **2** (1985), 189 (*Proc. Image Science'85*, Helsinki).
[2] BALLY G. von [Ed.] *Holography in Medicine and Biology*, Springer–Verlag, Berlin 1979.
[3] KASPRZAK H., PODBIELSKA H., BALLY G. von, SPIE **1026** (1988).
[4] SILVENNOINEN R., NYGRÉN K., KÄMÄ M., Opt. Eng. **31** (192), 1690.
[5] BUSKIRK V. C. von, ASHMAN R. B., *The elastic moduli of bone*, [In] *Mechanical Properties of Bone*, [Ed.] S. C. Cowin, Tulane University, 1981.
[6] EVANS F., *Mechanical Properties of Bone*, Charles Thomes Publ., Spriengfield 1973.
[7] PIZIALI R. L., HIGHT T. K., NAGEL D. A., J. Biomech. **13** (1980), 881.
[8] MILLER G. J., PURKEY W. W., Jr., J. Biomech. **13** (1980), 1.
[9] LEVIS J. L., J. Biomech. **8** (1975), 17.
[10] PIOTROWSKI G., WILCOX G. A., J. Biomech. **4** (1971), 497.
[11] RYBICKI E. F., SIMONEN F. A., WEISS E. B., J. Biomech. **5** (1972), 203.

Received April 4, 1994